



Search for $D^0\text{-}\bar{D}^0$ mixing in $D^0 \rightarrow K^+\pi^-$ decays and measurement of the doubly-Cabibbo-suppressed decay rate

J. Li,³¹ Z. P. Zhang,³¹ A. J. Schwartz,⁴ K. Abe,⁸ K. Abe,³⁷ H. Aihara,³⁹ M. Akatsu,²⁰ Y. Asano,⁴³ T. Aushev,¹² A. M. Bakich,³⁴ A. Bay,¹⁶ I. Bedny,¹ U. Bitenc,¹³ I. Bizjak,¹³ A. Bondar,¹ A. Bozek,²⁵ M. Bračko,^{18,13} J. Brodzicka,²⁵ T. E. Browder,⁷ Y. Chao,²⁴ A. Chen,²² K.-F. Chen,²⁴ W. T. Chen,²² B. G. Cheon,³ R. Chistov,¹² S.-K. Choi,⁶ Y. Choi,³³ A. Chuvikov,³⁰ S. Cole,³⁴ J. Dalseno,¹⁹ M. Danilov,¹² M. Dash,⁴⁴ L. Y. Dong,¹⁰ A. Drutskoy,⁴ S. Eidelman,¹ V. Eiges,¹² Y. Enari,²⁰ F. Fang,⁷ S. Fratina,¹³ N. Gabyshev,¹ A. Garmash,³⁰ T. Gershon,⁸ G. Gokhroo,³⁵ J. Haba,⁸ K. Hayasaka,²⁰ H. Hayashii,²¹ M. Hazumi,⁸ T. Higuchi,⁸ T. Hokuue,²⁰ Y. Hoshi,³⁷ S. Hou,²² W.-S. Hou,²⁴ T. Iijima,²⁰ A. Imoto,²¹ K. Inami,²⁰ R. Itoh,⁸ M. Iwasaki,³⁹ Y. Iwasaki,⁸ J. H. Kang,⁴⁵ J. S. Kang,¹⁴ S. U. Kataoka,²¹ N. Katayama,⁸ H. Kawai,² T. Kawasaki,²⁷ H. R. Khan,⁴⁰ J. H. Kim,³³ S. K. Kim,³² K. Kinoshita,⁴ P. Krokovny,¹ R. Kulasiri,⁴ C. C. Kuo,²² Y.-J. Kwon,⁴⁵ J. S. Lange,⁵ G. Leder,¹¹ S. H. Lee,³² T. Lesiak,²⁵ A. Limosani,¹⁹ S.-W. Lin,²⁴ D. Liventsev,¹² J. MacNaughton,¹¹ G. Majumder,³⁵ F. Mandl,¹¹ T. Matsumoto,⁴¹ A. Matyja,²⁵ W. Mitaroff,¹¹ H. Miyata,²⁷ R. Mizuk,¹² D. Mohapatra,⁴⁴ T. Mori,⁴⁰ T. Nagamine,³⁸ Y. Nagasaka,⁹ T. Nakadaira,³⁹ E. Nakano,²⁸ S. Nishida,⁸ O. Nitoh,⁴² S. Ogawa,³⁶ T. Ohshima,²⁰ S. L. Olsen,⁷ W. Ostrowicz,²⁵ H. Ozaki,⁸ P. Pakhlov,¹² H. Palka,²⁵ H. Park,¹⁵ N. Parslow,³⁴ L. S. Peak,³⁴ L. E. Pilonen,⁴⁴ H. Sagawa,⁸ Y. Sakai,⁸ N. Sato,²⁰ T. Schietinger,¹⁶ O. Schneider,¹⁶ P. Schönmeier,³⁸ J. Schümann,²⁴ C. Schwanda,¹¹ S. Semenov,¹² K. Senyo,²⁰ M. E. Sevier,¹⁹ H. Shibuya,³⁶ V. Sidorov,¹ A. Somov,⁴ N. Soni,⁴⁶ R. Stamen,⁸ S. Stanič,^{43,*} M. Starič,¹³ T. Sumiyoshi,⁴¹ S. Y. Suzuki,⁸ O. Tajima,⁸ F. Takasaki,⁸ K. Tamai,⁸ N. Tamura,²⁷ M. Tanaka,⁸ G. N. Taylor,¹⁹ Y. Teramoto,²⁸ X. C. Tian,²⁹ T. Tsuboyama,⁸ T. Uglov,¹² K. Ueno,²⁴ S. Uno,⁸ G. Varner,⁷ S. Villa,¹⁶ C. C. Wang,²⁴ C. H. Wang,²³ B. D. Yabsley,⁴⁴ A. Yamaguchi,³⁸ H. Yamamoto,³⁸ Y. Yamashita,²⁶ Heyoung Yang,³² J. Ying,²⁹ Y. Yuan,¹⁰ Y. Yusa,³⁸ S. L. Zang,¹⁰ C. C. Zhang,¹⁰ J. Zhang,⁸ L. M. Zhang,³¹ Z. Zheng,¹⁰ and D. Žontar^{17,13}

(The Belle Collaboration)

¹*Budker Institute of Nuclear Physics, Novosibirsk*

²*Chiba University, Chiba*

³*Chonnam National University, Kwangju*

⁴*University of Cincinnati, Cincinnati, Ohio 45221*

⁵*University of Frankfurt, Frankfurt*

⁶*Gyeongsang National University, Chinju*

⁷*University of Hawaii, Honolulu, Hawaii 96822*

⁸*High Energy Accelerator Research Organization (KEK), Tsukuba*

- ⁹*Hiroshima Institute of Technology, Hiroshima*
¹⁰*Institute of High Energy Physics, Chinese Academy of Sciences, Beijing*
¹¹*Institute of High Energy Physics, Vienna*
¹²*Institute for Theoretical and Experimental Physics, Moscow*
¹³*J. Stefan Institute, Ljubljana*
¹⁴*Korea University, Seoul*
¹⁵*Kyungpook National University, Taegu*
¹⁶*Swiss Federal Institute of Technology of Lausanne, EPFL, Lausanne*
¹⁷*University of Ljubljana, Ljubljana*
¹⁸*University of Maribor, Maribor*
¹⁹*University of Melbourne, Victoria*
²⁰*Nagoya University, Nagoya*
²¹*Nara Women's University, Nara*
²²*National Central University, Chung-li*
²³*National United University, Miao Li*
²⁴*Department of Physics, National Taiwan University, Taipei*
²⁵*H. Niewodniczanski Institute of Nuclear Physics, Krakow*
²⁶*Nihon Dental College, Niigata*
²⁷*Niigata University, Niigata*
²⁸*Osaka City University, Osaka*
²⁹*Peking University, Beijing*
³⁰*Princeton University, Princeton, New Jersey 08545*
³¹*University of Science and Technology of China, Hefei*
³²*Seoul National University, Seoul*
³³*Sungkyunkwan University, Suwon*
³⁴*University of Sydney, Sydney NSW*
³⁵*Tata Institute of Fundamental Research, Bombay*
³⁶*Toho University, Funabashi*
³⁷*Tohoku Gakuin University, Tagajo*
³⁸*Tohoku University, Sendai*
³⁹*Department of Physics, University of Tokyo, Tokyo*
⁴⁰*Tokyo Institute of Technology, Tokyo*
⁴¹*Tokyo Metropolitan University, Tokyo*
⁴²*Tokyo University of Agriculture and Technology, Tokyo*
⁴³*University of Tsukuba, Tsukuba*
⁴⁴*Virginia Polytechnic Institute and State University, Blacksburg, Virginia 24061*
⁴⁵*Yonsei University, Seoul*
⁴⁶*Panjab University, Chandigarh*

Abstract

We have searched for mixing in the D^0 - \overline{D}^0 system by measuring the decay-time distribution of $D^0 \rightarrow K^+\pi^-$ decays. The analysis uses 90 fb^{-1} of data collected by the Belle detector at the KEKB e^+e^- collider. We fit the decay-time distribution for the mixing parameters x' and y' and also for the parameter R_D , which is the ratio of the rate for the doubly-Cabibbo-suppressed decay $D^0 \rightarrow K^+\pi^-$ to that for the Cabibbo-favored decay $D^0 \rightarrow K^-\pi^+$. We do these fits both assuming CP conservation and allowing for CP violation. We use a frequentist method to obtain a 95% C.L. region in the x'^2 - y' plane. Assuming no mixing, we measure $R_D = (0.381 \pm 0.017^{+0.008}_{-0.016})\%$.

PACS numbers: 12.15.Ff, 13.25.Ft, 11.30.Er

The phenomenon of mixing among quark flavors has been observed in the $K^0\text{-}\bar{K}^0$ and $B^0\text{-}\bar{B}^0$ systems but not yet in the $D^0\text{-}\bar{D}^0$ system. The rate for $D^0\text{-}\bar{D}^0$ mixing within the Standard Model (SM) is small, typically well below experimental upper limits [1]. Observation of mixing much larger than this expectation could indicate new physics, such as a $\Delta C=2$ interaction. Such nonstandard processes may also give rise to CP -violating effects.

In this paper we present a search for $D^0\text{-}\bar{D}^0$ mixing and CP violation (CPV) in mixing with greater sensitivity than that of previous searches. The data sample consists of 90 fb^{-1} recorded by the Belle experiment at the KEKB asymmetric e^+e^- collider [2]. The Belle detector [3] consists of a three-layer silicon vertex detector (SVD), a 50-layer central drift chamber (CDC), an array of aerogel threshold Cherenkov counters (ACC), time-of-flight scintillation counters (TOF), and an electromagnetic calorimeter comprised of CsI(Tl) crystals. These detectors are located within a solenoid coil providing a 1.5 T magnetic field. An iron flux-return outside the coil is instrumented to identify muons and K_L^0 mesons.

The dominant two-body decay of the D^0 is the Cabibbo-favored (CF) decay $D^0 \rightarrow K^-\pi^+$ [4]. We search for mixing by reconstructing the “wrong-sign” decay $D^0 \rightarrow K^+\pi^-$, which would arise from a D^0 mixing to \bar{D}^0 and subsequently decaying via $\bar{D}^0 \rightarrow K^+\pi^-$. The flavor of the D is identified by requiring that it originate from $D^{*+} \rightarrow D^0\pi^+$ or $D^{*-} \rightarrow \bar{D}^0\pi^-$ and noting the charge of the accompanying pion. In addition to arising via mixing, $D^0 \rightarrow K^+\pi^-$ can also occur via a doubly-Cabibbo-suppressed (DCS) amplitude. The two processes can be distinguished via the decay-time distribution. This method has been used by FNAL E791 [5], CLEO [6], and BaBar [7] to search for mixing and measure or constrain the DCS decay rate.

The parameters used to characterize mixing are $x \equiv \Delta m/\bar{\Gamma}$ and $y \equiv \Delta\Gamma/(2\bar{\Gamma})$, where Δm and $\Delta\Gamma$ are the differences in mass and decay width between the two $D^0\text{-}\bar{D}^0$ mass eigenstates, and $\bar{\Gamma}$ is the mean decay width. For $|x|, |y| \ll 1$ and negligible CPV , the decay time distribution for $D^0 \rightarrow K^+\pi^-$ can be expressed as

$$\frac{dN}{dt} \propto e^{-\bar{\Gamma}t} \left[R_D + \sqrt{R_D} y'(\bar{\Gamma}t) + \frac{x'^2 + y'^2}{4} (\bar{\Gamma}t)^2 \right], \quad (1)$$

where R_D is the ratio of DCS to CF decay rates, $x' = x \cos \delta + y \sin \delta$, $y' = y \cos \delta - x \sin \delta$, and δ is the strong phase difference between the DCS and CF amplitudes. The first term in brackets is due to the DCS amplitude, the last term is due to mixing, and the middle term is due to interference between the two processes. The time-integrated rate for $D^0 \rightarrow K^+\pi^-$ relative to that for $D^0 \rightarrow K^-\pi^+$ is $R_D + \sqrt{R_D} y' + (x'^2 + y'^2)/2$.

To allow for CP violation, we follow Ref. [7] and apply Eq. (1) to D^0 and \bar{D}^0 decays separately. This results in six observables: $\{R_D^+, x'^{+2}, y'^{+}\}$ for D^0 and $\{R_D^-, x'^{-2}, y'^{-}\}$ for \bar{D}^0 . CP violation is parametrized by the asymmetries $A_D = (R_D^+ - R_D^-)/(R_D^+ + R_D^-)$ and $A_M = (R_M^+ - R_M^-)/(R_M^+ + R_M^-)$, where $R_M^\pm = (x'^{\pm 2} + y'^{\pm 2})/2$. The asymmetry A_D characterizes CPV in the DCS decay amplitude, and A_M characterizes CPV in $D^0\text{-}\bar{D}^0$ mixing. The observables are related to x' and y' via

$$x'^{\pm} = \left[\frac{1 \pm A_M}{1 \mp A_M} \right]^{\frac{1}{4}} (x' \cos \phi \pm y' \sin \phi) \quad (2)$$

$$y'^{\pm} = \left[\frac{1 \pm A_M}{1 \mp A_M} \right]^{\frac{1}{4}} (y' \cos \phi \mp x' \sin \phi), \quad (3)$$

where ϕ is a weak phase and characterizes CPV occurring via interference between mixed and unmixed decay amplitudes. Note that x'^{\pm} , y'^{\pm} are unchanged by the transformation $x' \rightarrow -x'$, $y' \rightarrow -y'$, and $\phi \rightarrow \phi + \pi$; thus for definiteness we restrict ϕ to the range $|\phi| < \pi/2$.

We select $D^0 \rightarrow K^- \pi^+$ decays by requiring two oppositely-charged tracks, with at least four SVD hits, that satisfy K and π identification criteria. These criteria are $\mathcal{L}_K > 0.6$ and $\mathcal{L}_\pi > 0.4$, where \mathcal{L} is the relative likelihood for a track to be a K or π based on dE/dx information in the CDC and the responses of the TOF and ACC systems. These criteria have efficiencies of 88.0% and 88.5% and π/K misidentification rates of 8.5% and 8.8%, respectively. We combine the D^0 candidate with a low-momentum pion (π_{slow}) to form a $D^{*+} \rightarrow D^0 \pi^+$ candidate. Candidates in which the charge of π_{slow} is opposite (equal to) that of the K^\pm are referred to as “right-sign” or RS (“wrong-sign” or WS) decays. To reject WS background from $D^0 \rightarrow K^- \pi^+$ in which the K is misidentified as π and the π is misidentified as K , we recalculate $m_{K\pi}$ with the K and π assignments swapped and reject events with $|m_{K\pi} - m_{D^0}| < 28 \text{ MeV}/c^2$. To eliminate D^{*+} ’s from B decays, we require $p_{D^*} > 2.5 \text{ GeV}/c$, where p_{D^*} is evaluated in the e^+e^- center-of-mass frame.

The D^0 vertex is obtained by fitting the daughter K/π tracks. The D^* vertex is taken as the intersection of the D^0 momentum vector with the interaction profile region. We require a good χ^2 for each vertex fit. The momentum of π_{slow} is refitted with the constraint that it originates from the D^* vertex. The D^0 decay time is calculated as $(\ell_{D^0}/p_{D^0}) \times m_{D^0}$, where ℓ_{D^0} is the distance between the D^0 and D^* vertices projected onto the \vec{p}_{D^0} direction. The decay-time resolution is typically 0.2 ps.

We measure R_D , x'^2 , and y' of Eq. (1) via an unbinned maximum likelihood fit to the WS decay-time distribution. The likelihood function consists of probability density functions (pdf’s) for signal and several backgrounds. The pdf’s depend on the decay time, the mass $m_{K\pi}$, and the kinetic energy released $Q \equiv m_{K\pi\pi_{\text{slow}}} - m_{K\pi} - m_\pi$. The latter equals only 5.85 MeV/ c^2 for $D^{*+} \rightarrow D^0 \pi_{\text{slow}}^+ \rightarrow K\pi\pi_{\text{slow}}^+$ decays, which is near the threshold.

The signal pdf for event i is smeared by a resolution function $R_i = (1 - f_{\text{tail}}) G(t_i - t', \sigma_{t,i}; \mu, S) + f_{\text{tail}} G(t_i - t', \sigma_{t,i}; \mu, S_{\text{tail}})$, where the G ’s are Gaussians with common mean μ and standard deviations $(S \times \sigma_{t,i})$ and $(S_{\text{tail}} \times \sigma_{t,i})$, and $\sigma_{t,i}$ is the uncertainty in decay time t for event i . The parameters f_{tail} , μ , and scaling factors S and S_{tail} are determined from data. The background pdf’s are smeared by similar resolution functions (see below). To check the resolution function, we fit the RS sample in the same manner as the WS sample except that the signal pdf has a purely exponential time dependence.

There are four backgrounds to the WS sample: (a) random π background, in which a random π^+ is paired with a $\bar{D}^0 \rightarrow K^+ \pi^-$ decay (the pdf is peaked in $m_{K\pi}$ but broad in Q); (b) $D^{*+} \rightarrow D^0 \pi^+$ followed by D^0 decaying to ≥ 3 -body final states (the pdf is broad in $m_{K\pi}$ and broad but enhanced in Q); (c) D^+/D_s^+ decays; and (d) combinatorial. We determine the level of each background by performing a two-dimensional fit to the $m_{K\pi}$ - Q distribution. When fitting the RS sample, the $m_{K\pi}$ and Q means and widths for signal are floated; when fitting the WS sample, these means and widths are fixed to the values obtained from the RS fit. Also for the WS fit, the ratio of D^+/D_s^+ to ≥ 3 -body backgrounds is fixed to the value obtained from Monte Carlo (MC) simulation. The RS fit finds $227\,721 \pm 497$ $D^0 \rightarrow K^- \pi^+$ decays, and the WS fit finds 845 ± 40 $D^0 \rightarrow K^+ \pi^-$ decays. The ratio $R_{\text{WS}} \equiv \Gamma(D^0 \rightarrow K^+ \pi^-)/\Gamma(D^0 \rightarrow K^- \pi^+) = (0.371 \pm 0.018)\%$ (statistical errors only). The ratio of WS signal to background is 0.9; the latter is mostly random π (59%) and combinatorial (36%). The WS $m_{K\pi}$ and Q distributions are shown in Fig. 1 along with the fit projections.

To fit the decay-time distributions of RS and WS samples, we consider the 4σ region

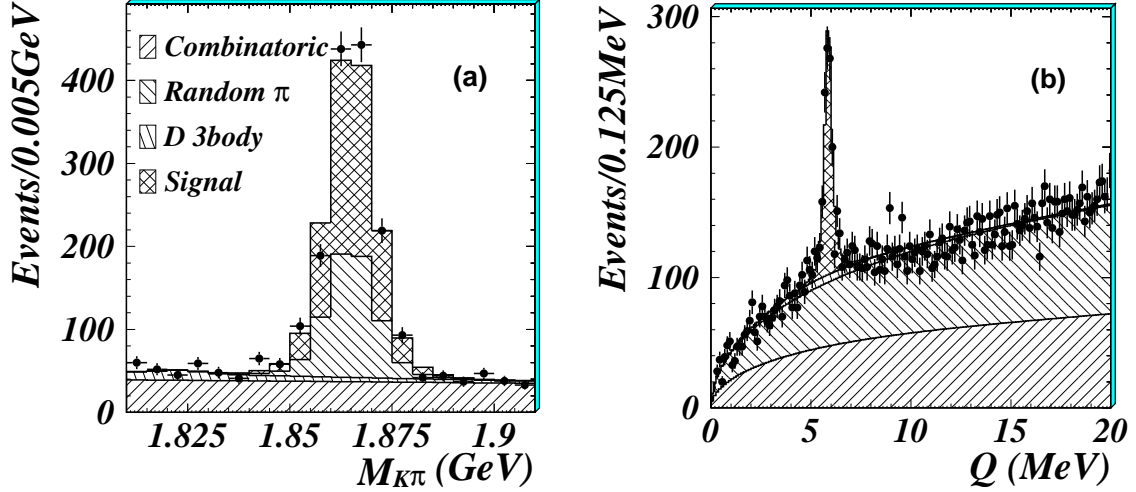


FIG. 1: Distributions of (a) WS $m_{K\pi}$ with $|Q - 5.9 \text{ MeV}| < 0.6 \text{ MeV}$; and (b) WS Q with $|m_{K\pi} - m_{D^0}| < 20 \text{ MeV}/c^2$. Superimposed on the data (points with error bars) are projections of the $m_{K\pi}$ - Q fit.

$|m_{K\pi} - m_{D^0}| < 22 \text{ MeV}/c^2$ and $|Q - 5.9 \text{ MeV}| < 1.5 \text{ MeV}/c^2$. The signal and background yields (which normalize the pdf's in the likelihood function) are determined from the $m_{K\pi}$ - Q fit described above. The decay-time distributions for the backgrounds before smearing are taken to be: $e^{-t/\tau_{D^0}}$ for random π background, $e^{-t/\tau_{D^{3b}}}$ for ≥ 3 -body D^0 background, $e^{-t/\tau_{D^{ch}}}$ for D^+/D_s^+ background, and $\delta(t)$ for combinatorial background. Parameter $\tau_{D^{3b}}$ is obtained from fitting sideband data, and $\tau_{D^{ch}}$ is obtained from MC simulation. These time distributions are convolved with resolution functions. For random- π background (and the small multi-body $D^0/D^+/D_s^+$ background), the resolution function used is the same as that for signal; for combinatorial background, the resolution function has the same form but parameters $f_{\text{tail}}^{(\text{comb})}$, $S^{(\text{comb})}$, $S_{\text{tail}}^{(\text{comb})}$ are determined from fitting sideband data.

The fitting procedure is implemented in steps as follows. We first fit the RS signal region using a simple background model to obtain a first estimate of signal resolution function parameters. We use this resolution function to fit an RS sideband region, which yields $f_{\text{tail}}^{(\text{comb})}$, $S^{(\text{comb})}$, $S_{\text{tail}}^{(\text{comb})}$, and $\tau_{D^{3b}}$ for RS background. We then fit the RS signal region with these parameters fixed, which yields μ , f_{tail} , S , S_{tail} and, as a check, τ_{D^0} . We subsequently use this resolution function to fit the WS sideband region, obtaining $f_{\text{tail}}^{(\text{comb})}$, $S^{(\text{comb})}$, $S_{\text{tail}}^{(\text{comb})}$, and $\tau_{D^{3b}}$ for WS background. Finally, we fit the WS signal region, fixing these background parameters and those of the signal resolution function; this yields R_D , x'^2 , and y' .

The above fitting procedure has undergone several checks. In MC simulation, background parameters obtained from the sideband region fit describe well the background in the signal region. The resolution function obtained from data is very similar to that obtained from the MC. The lifetime τ_{D^0} obtained from the RS signal region fit is $415.1 \pm 1.4 \text{ fs}$, consistent with the PDG value [8]; the χ^2 of the fit projection is 56.0 for 55 bins. We generated MC samples having the same size as the data sample, adding the corresponding amount of background, and repeated the fitting procedure. For nine sets of (x'^2, y') values (spanning the ranges $[0, 2] \times 10^{-3}$ and $[-2, 2] \times 10^{-2}$, respectively), the fit recovers values consistent with the generated values. For these sets we also generated ensembles of “toy” MC experiments, i.e., without detector simulation, and smeared the time distributions appropriately. Fitting

these experiments shows negligible fit bias.

To this point in the analysis, all optimization of selection criteria was done “blindly,” i.e., without fitting WS signal events. We now fix the criteria and fit this sample. Four fits are done, yielding the results listed in Table I. For the first fit we require that CP be conserved. The projection of this fit superimposed on the data is shown in Fig. 2; the χ^2 of the projection is 71.9 for 60 bins. The central value for x'^2 is negative (i.e., outside the physical region); thus the most-likely value is zero, and we refit the data fixing $x'^2 = 0$. The χ^2 of this fit projection is 73.2 for 60 bins, which is satisfactory. The y' value is $\sim 2\sigma$ from zero; when we generate MC experiments with this value (and $x'^2=0$), we find that the probability of obtaining an x'^2 value as negative as what we measure in the data is 8%. For the third fit we allow for CPV and fit the $D^0 \rightarrow K^+ \pi^-$ and $\bar{D}^0 \rightarrow K^- \pi^+$ samples separately. For R_D^+ and R_D^- we obtain $(0.255^{+0.058}_{-0.056})\%$ and $(0.324 \pm 0.052)\%$, respectively. We calculate A_D and A_M and use Eqs. (2) and (3) to solve for x'^2 and y' . Finally, for the last fit we assume no mixing or CPV and set $x'^2 = y' = 0$; the χ^2 of this fit projection is 75.6 for 60 bins, somewhat worse than for the case of mixing.

TABLE I: Summary of results from the separate likelihood fits. The 95% CL intervals are obtained from a frequentist method (see text) and include systematic errors.

Fit Case	Parameter	Fit Result ($\times 10^{-3}$)	95% CL interval ($\times 10^{-3}$)
No CPV	x'^2	$-1.53^{+0.80}_{-1.00}$	$x'^2 < 0.81$
	y'	$25.4^{+11.1}_{-10.2}$	$-8.2 < y' < 16$
	R_D	2.87 ± 0.37	$2.7 < R_D < 4.0$
	R_M	–	$R_M < 0.42$
No CPV $x' = 0$ (fixed)	y'	6.0 ± 3.3	–
	R_D	3.43 ± 0.26	–
CPV allowed	A_D	-80 ± 77	$-250 < A_D < 110$
	A_M	987^{+13}_{-380}	$-991 < A_M < 1000$
	x'^2	–	$x'^2 < 0.89$
	y'	–	$-30 < y' < 27$
	R_M	–	$R_M < 0.46$
No mixing or CPV	R_D	3.81 ± 0.17 (stat.) $^{+0.08}_{-0.16}$ (syst.)	

To obtain 95% CL limits on x'^2 and y' , we use a frequentist method (similar to that used in Ref. [7]) with Feldman-Cousins ordering [9]. For points $\vec{\alpha} = (x'^2, y')$, we generate ensembles of toy MC experiments and fit them using the same procedure as that used for the data. For each experiment we record the difference in likelihood $\Delta L = \ln L_{\max} - \ln L(\vec{\alpha})$, where L_{\max} is evaluated for $x'^2 \geq 0$. The locus of points $\vec{\alpha}$ for which 95% of the ensemble has ΔL less than that of the data is taken as the 95% CL contour. This contour is shown in Fig. 3.

To allow for CPV , we obtain separate $1 - \sqrt{0.05} = 77.6\%$ CL contours for (x'^{+2}, y'^{+}) and (x'^{-2}, y'^{-}) . We combine points on the (x'^{+2}, y'^{+}) contour with points on the (x'^{-2}, y'^{-}) contour and use these values to solve Eqs. (2) and (3) for x'^2 and y' . Because the relative sign of x'^{+} and x'^{-} is unknown, there are two solutions (one for each sign); we plot both

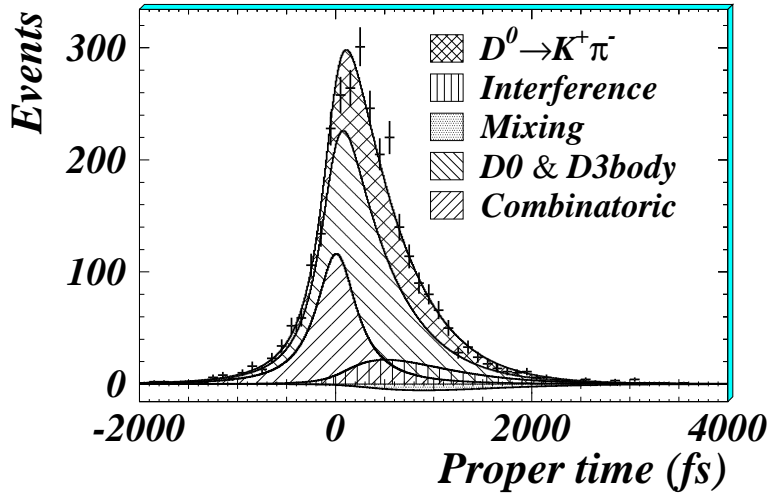


FIG. 2: The decay-time distribution for WS events satisfying $|m_{K\pi} - m_{D^0}| < 22 \text{ MeV}/c^2$ and $|Q - 5.9 \text{ MeV}| < 1.5 \text{ MeV}$. Superimposed on the data (points with error bars) are projections of the decay-time fit.

in the (x'^2, y') plane and take the outermost envelope of points to be the 95% CL contour allowing for CPV . This contour has a complicated shape due to the two solutions. Because the contour includes the point $x'^2 = y' = 0$, we cannot constrain ϕ at this C.L.

We evaluate systematic errors by varying parameters used to select and fit the data within their uncertainties and recording the new fit values $\vec{\alpha}_{\text{new}}$ obtained. These values are shifted with respect to the original central value $\vec{\alpha}_0$. We find the significance m of a shift via the formula $m^2 = -2[\ln L(\vec{\alpha}_{\text{new}}) - \ln L(\vec{\alpha}_0)]/2.30$, where the factor 2.30 corresponds to 68.3% confidence in two dimensions. We add in quadrature the significances of individual shifts to obtain an overall scaling factor $\sqrt{1 + \sum m_i^2}$. We increase the 95% CL statistical contour by this factor to include systematic errors. As a check, we generate an ensemble of toy MC experiments with $\vec{\alpha}_{\text{MC}} = (0., 0.006)$ and fit them to confirm that 68.3% of the ensemble satisfies $-2[\ln L(\vec{\xi}) - \ln L(\vec{\alpha}_{\text{MC}})] < 2.3$, where $\vec{\xi}$ is the central value for an experiment.

The parameters varied include kaon and pion identification criteria, the allowed χ^2 of the vertex fit, background shape and normalization parameters, and resolution function parameters for both signal and combinatorial background. The largest shift in (x'^2, y') occurs for the D^{*+} momentum cut; when this is varied over a significant range, $(\Delta x'^2/x'^2)_{\text{max}} = 12\%$, $(\Delta y'/y')_{\text{max}} = 10\%$, and $\Delta(-2 \ln L) = 0.092$. The overall scaling factor is $\sqrt{1 + \sum m_i^2} = 1.08$. For the general case allowing for CPV , we scale the D^0 and \bar{D}^0 contours separately before combining. The rescaled 95% CL contours are shown in Fig. 3: the dashed contour corresponds to the CP -conserving case and the solid contour to the general case. Projecting these contours onto the coordinate axes gives the 95% CL intervals for x'^2 and y' listed in Table I.

In summary, we have searched for D^0 - \bar{D}^0 mixing and CP violation using WS $D^0 \rightarrow K^+ \pi^-$ decays. In 90 fb^{-1} of data we find no evidence for these processes and constrain the mixing parameters x'^2 and y' and the CP asymmetry parameters A_D and A_M . The limits for x'^2 and y' are more stringent than previous results; the value for R_D (the ratio of DCS to CF decays) has smaller uncertainty.

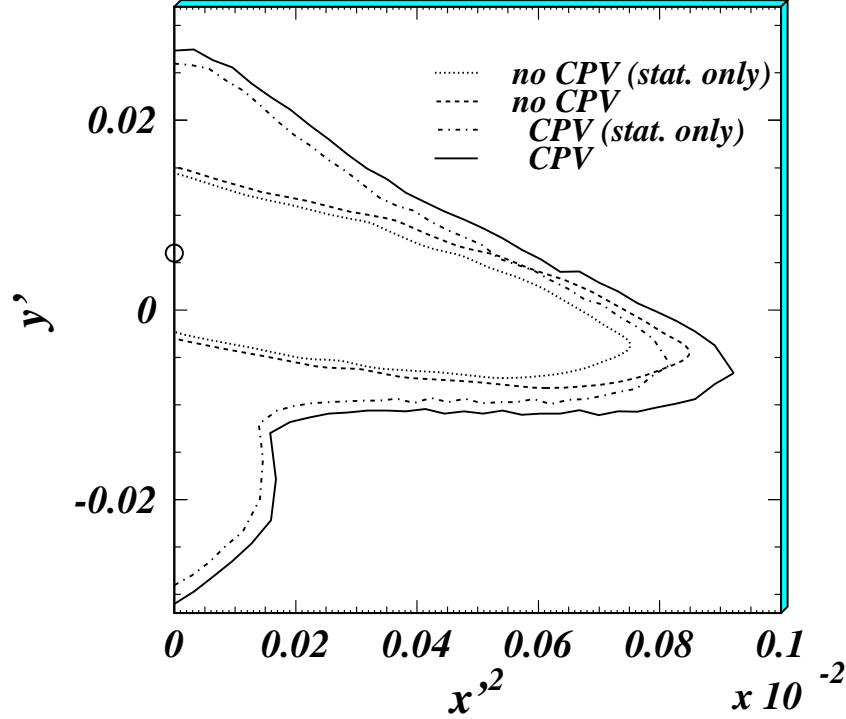


FIG. 3: 95% CL regions for (x'^2, y') . The dotted (dashed) contour is statistical (statistical and systematic) and corresponds to CP conservation. The dash-dotted (solid) contour is statistical (statistical and systematic) and allows for CPV . The open circle represents the most-likely value when CP is conserved and x'^2 is constrained to be ≥ 0 .

We thank the KEKB group for the excellent operation of the accelerator, the KEK cryogenics group for the efficient operation of the solenoid, and the KEK computer group and the NII for valuable computing and Super-SINET network support. We acknowledge support from MEXT and JSPS (Japan); ARC and DEST (Australia); NSFC (contract No. 10175071, China); DST (India); the BK21 program of MOEHRD and the CHEP SRC program of KOSEF (Korea); KBN (contract No. 2P03B 01324, Poland); MIST (Russia); MESS (Slovenia); NSC and MOE (Taiwan); and DOE (USA).

* on leave from Nova Gorica Polytechnic, Nova Gorica

- [1] For a comprehensive review see S. Bianco, F.L. Fabbri, D. Benson, and I. Bigi, Riv. Nuovo Cim. **26N7-8**, 1 (2003). See also A. Falk *et al.*, Phys. Rev. D **69**, 114021 (2004).
- [2] S. Kurokawa and E. Kikutani, Nucl. Instr. Meth. A **499**, 1 (2003).
- [3] A. Abashian *et al.* (Belle), Nucl. Instr. Meth. A **479**, 117 (2002).
- [4] Charge-conjugate modes are included throughout this paper unless noted otherwise.
- [5] E. Aitala *et al.* (E791), Phys. Rev. D **57**, 13 (1998).
- [6] R. Godang *et al.* (CLEO), Phys. Rev. Lett. **84**, 5038 (2000).
- [7] B. Aubert *et al.* (BaBar), Phys. Rev. Lett. **91**, 171801 (2003).
- [8] S. Eidelman *et al.* (PDG), Phys. Lett. B **592**, 1 (2004).
- [9] G. J. Feldman and R. D. Cousins, Phys. Rev. D **57**, 3873 (1998).